Nonlinear symmetry breaking of Aharonov-Bohm cages

Goran Gligorić,[1] Petra P. Beličev,[1] Daniel Leykam,[2] and Aleksandra Maluckov[1]
[1]*P* Group, Vinča Institute of Nuclear Sciences, University of Belgrade, P.O. Box 522, 11001 Belgrade, Serbia*
[2]*Center for Theoretical Physics of Complex Systems, Institute for Basic Science, Daejeon 34126, Republic of Korea*

(Received 11 October 2018; published 15 January 2019)

We study the influence of mean-field cubic nonlinearity on Aharonov-Bohm caging in a diamond lattice with synthetic magnetic flux. For sufficiently weak nonlinearities, the Aharonov-Bohm caging persists as periodic nonlinear breathing dynamics. Above a critical nonlinearity, symmetry breaking induces a sharp transition in the dynamics and enables stronger wave-packet spreading. This transition is distinct from other flatband networks, where continuous spreading is induced by effective nonlinear hopping or resonances with delocalized modes and is in contrast to the quantum limit, where two-particle hopping enables arbitrarily large spreading. This nonlinear symmetry-breaking transition is readily observable in femtosecond laser-written waveguide arrays.

DOI: 10.1103/PhysRevA.99.013826

I. INTRODUCTION

Perfect wave localization emerges in certain noninteracting tight-binding networks via application of a fine-tuned magnetic flux [1,2]. The localization mechanism in such "Aharonov-Bohm (AB) cages" is the flux-controlled destructive interference between different propagation paths [3,4], which are recombined and forced to interfere at bottlenecks in the network. What is perhaps most interesting about AB caging is that this perfect localization is not limited to excitations at a precise energy (i.e., of a flat Bloch band); it persists for arbitrary initial states. This requires not just fine tuning, but also a network topology supporting closed flux-encircling plaquettes, leading to novel topological invariants and edge states [5–7].

First observed in a two-dimensional "dice" superconducting network nearly 20 years ago [8], recent advances in synthetic gauge-field engineering have renewed interest in AB caging in the context of quasi one- and two-dimensional mesoscopic networks, including quantum rings [9–11], Josephson junction arrays [12–16], optical lattices [17,18], and coupled optical waveguides [7,19–21], motivated by the goal of enhancing interaction effects. In particular, single-particle (noninteracting) eigenstates in AB cages are compactly localized but nonorthogonal, such that interactions induce two-particle hopping processes. This destroys the caging, leading to delocalized bound pairs, novel strongly correlated quantum phases such as $4e$ superconductivity, and time-reversal symmetry-breaking ground states [22–31].

Here we study AB caging in the presence of mean-field interactions described by the discrete nonlinear Schrödinger equation, relevant to Bose-Einstein condensates [32] and high-power light propagation in optical waveguide arrays [33], where AB caging was very recently observed [7,21]. Due to nonorthogonality of the compact localized eigenstates (CLS), weak nonlinearities are already sufficient to induce linear instabilities via coupling between neighboring CLS [34]. We demonstrate through numerical simulations that these instabilities are weak in the sense that the dynamics remain (quasi-)periodic and spreading to more distant lattice sites remains negligible; most of the power remains confined to the initially excited CLS as a stable breathing mode. At a critical nonlinearity strength we observe a sharp transition in the dynamics at which this breather becomes unstable due to nonlinear symmetry breaking between the two legs of each plaquette. Leg-dependent nonlinear phase shifts can then break the AB cage, leading to delocalization beyond that allowed within the linear stability analysis (LSA). Interestingly, this transition is not specific to the AB cage limit but is also robust to detunings of the effective flux, suggesting it is rooted in the presence of bottlenecks. This nonlinearity-induced transition may be useful for nonlinear switching functionalities and is distinctly different from the quantum limit in which two particles already delocalize under weak interactions.

II. MODEL

We consider light propagation in the quasi-one-dimensional diamond chain lattice with synthetically introduced magnetic flux. The diamond lattice has bipartite symmetry [35] with three sites per unit cell: A, B, and C, as shown in Fig. 1(a). The A sites are fourfold connected with the nearest neighbors, forming bottlenecks, while the B and C sites make twofold connections with surrounding sites. Evolution of the optical field $\psi_n = (a_n, b_n, c_n)$ in the presence of on-site nonlinearity is governed by the discrete nonlinear Schrödinger equation,

$$\begin{aligned} i\partial_z a_n &= b_n e^{-i\Gamma/2} + b_{n-1} + c_n + c_{n-1}e^{-i\Gamma/2} - g|a_n|^2 a_n, \\ i\partial_z b_n &= a_n e^{i\Gamma/2} + a_{n+1} - g|b_n|^2 b_n, \\ i\partial_z c_n &= a_n + a_{n+1}e^{i\Gamma/2} - g|c_n|^2 c_n. \end{aligned} \tag{1}$$

Here z is the propagation distance (analogous to time), g is the nonlinearity strength, Γ is the flux [20,24], n is the unit-cell index, and we have normalized the coupling to unity without loss of generality. Total beam power $P = \sum_n (|a_n|^2 + |b_n|^2 + |c_n|^2)$ and the Hamiltonian are conserved quantities.

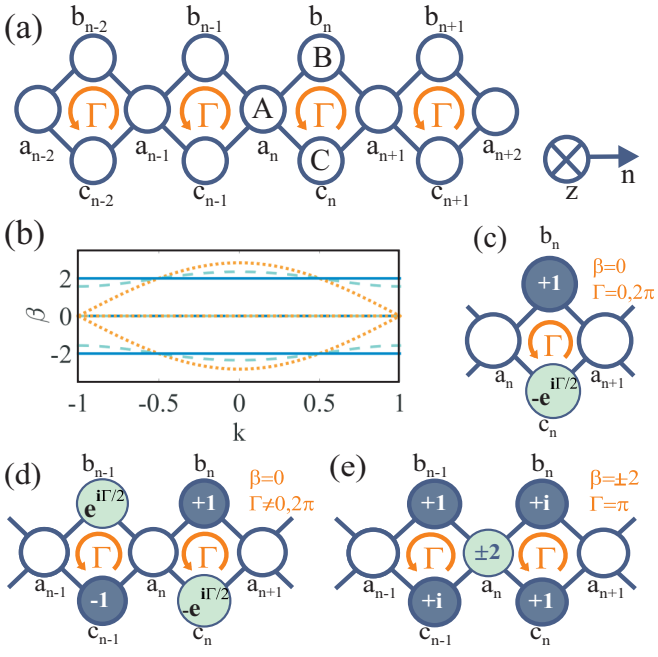

FIG. 1. (a) Schematic representation of a diamond lattice (characterized by bipartite symmetry) made of coupled optical waveguides. A synthetic magnetic flux Γ is applied in each plaquette. (b) Band structure for $\Gamma = 0, 2\pi$ (dotted orange line), $\Gamma = 3\pi/4$ (dashed turquoise line), and $\Gamma = \pi$ (blue solid lines). (c–e) Geometry-induced $\beta_{FB} = 0$ flatband modes for different flux strengths (c, d) and additional flatband modes ($\beta_{FB} = \pm 2$) originating due to the AB caging (e).

Experimentally, the flux Γ can be realized either through sinusoidal modulation of the refractive index of waveguides in z [20,21], or by implementation of an auxiliary waveguide with a carefully chosen refractive index in between two sites [7]. Both approaches may, in principle, affect the on-site nonlinear interaction terms which originate from optical Kerr nonlinearity of the bulk medium. For example, modulation of the waveguide depths may also perturb the effective nonlinear coefficient g (through modulation of the modal confinement). However, the recent experiments reported in Refs. [7,21] are based on weakly coupled arrays where these perturbations can be made negligible.

Specifically, Ref. [36] demonstrated the validity of a static nonlinear term in harmonically modulated waveguide arrays by comparing predictions of a tight-binding model similar to Eq. (1) against the more rigorous Schrödinger equation and experimental observations. With the auxiliary waveguide approach the fidelity of the emulation of the negative coupling is determined by the overlap of the linear eigenmodes with the auxiliary waveguides. The emulation becomes exact when the auxiliary waveguides are strongly detuned and this overlap tends to zero. The experiments of Ref. [37] achieved a fidelity of 99%, corresponding to an overlap of only 1%. Therefore, when linear AB caging is successfully implemented using this method, the nonlinearity of the auxiliary waveguides can be safely neglected and the our tight-binding model will accurately describe the propagation dynamics.

In the linear limit ($g = 0$), the Bloch wave eigenmodes are $\{a_n, b_n, c_n\} = (A, B, C)\exp(-i\beta z + ikn)$, where β and k denote the propagation constant and Bloch wave number, respectively. After its substitution into Eq. (1) we obtain the following dispersion relations:

$$\beta_{FB} = 0, \quad \beta_{\pm} = \pm 2\kappa\sqrt{1 + \cos(\Gamma/2)\cos(k)}.$$

The $\beta_{FB} = 0$ band is completely flat, regardless of the flux Γ, and is a consequence of the diamond network's topology (plaquettes coupled via bottleneck sites). The other bands are in general k dependent and only become flat in the AB cage limit $\Gamma = \pi$.

When $\Gamma = 0$ or 2π the flatband touches two surrounding dispersive bands at the Brillouin zone edge, as shown in Fig. 1(b). Figure 1(c) illustrates the fundamental CLS, which occupies two sites and is localized to a single unit cell. In general, when $\Gamma \neq 0, 2\pi$ the $\beta_{FB} = 0$ flatband is separated from the others by a gap, and the fundamental CLS occupying four sites is not orthogonal with neighboring CLSs, see Fig. 1(d) [38]. Meanwhile, in the AB cage limit the additional flatbands at $\beta = \pm 2\kappa$ host five-site CLS that also excite one of the bottleneck sites [Fig. 1(e)].

III. LINEAR STABILITY OF NONLINEAR CLS

We start by analyzing how nonlinearity can lead to instability of the CLS, and potentially induce transport. Our focus is on the $\beta_{FB} = 0$ CLS, which exists and can be continued as a nonlinear CLS, regardless of the synthetic magnetic flux strength. The general behavior of perturbed CLSs can be related to the eigenvalue (EV) spectra which are obtained via the LSA by applying a small perturbation p_n to the CLS profile ψ_n and linearizing the equations of motion, Eq. (1) [34,39]. The eigenvalues λ of the linearized equations of motion characterize the initial stage of instability development of CLS.

When $\Gamma \neq 0, 2\pi$, nonlinearity can induce coupling between neighboring nonorthogonal CLSs. This can be identified in the LSA spectrum via pure real EVs (exponential instabilities) in Fig. 2. The perturbation eigenmodes are compact and have vanishing tails in the AB cage limit ($\Gamma = \pi$), and are localized with exponential tails for other values of Γ. This source of instability only induces significant coupling between the very first neighboring CLSs originating from the same submanifold (same flatband). It cannot induce longer range spreading.

A typical spectrum of perturbed CLSs emerging from single gapped flatband located at $\beta_{FB} = 0$ is depicted in Fig. 2(a) for the case $\Gamma = 3\pi/4$. Even for small nonlinearity strengths g, the pure real EV branch is accompanied by quartets of complex EVs with nonzero real parts, indicating oscillatory instabilities arising due to coupling between the dispersive bands and the CLS. Since the dispersive states are delocalized, this mixing can induce spreading of energy through the entire lattice [34]. A similar scenario is obtained for $\Gamma = 0, 2\pi$.

On the other hand, for $\Gamma = \pi$ the pure real EV branches simultaneously occur with the complex EV quartets coming from the flatbands characterized with $\beta_{FB} = \pm 2$ [Fig. 2(b)], whose eigenmodes are also compact and localized. The

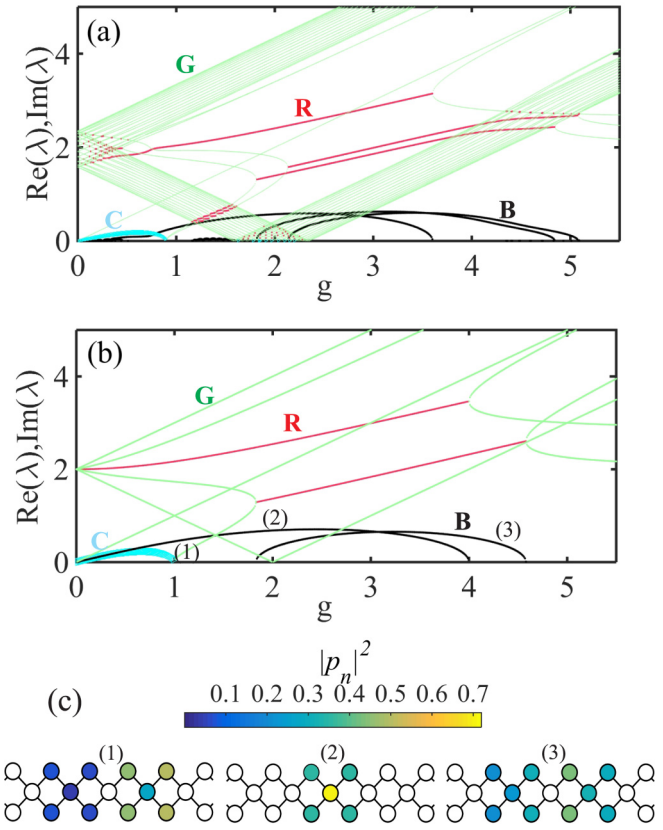

FIG. 2. Linear instability spectrum of nonlinear CLS. (a, b) Positive frequency part of full linear perturbation eigenvalue (EV) spectrum for (a) $\Gamma = 3\pi/4$ and (b) $\Gamma = \pi$. Pure real EVs (cyan – C) and nonzero real parts of complex EVs (black – B) mark regions of CLS linear instability. Pure imaginary EVs and imaginary parts of complex EVs are shown in green (G) and red (R), respectively. (c) Characteristic eigenmode profiles of perturbed CLS corresponding to three EV branches (1), (2), and (3) from (b). Size of the system is $N = 21$.

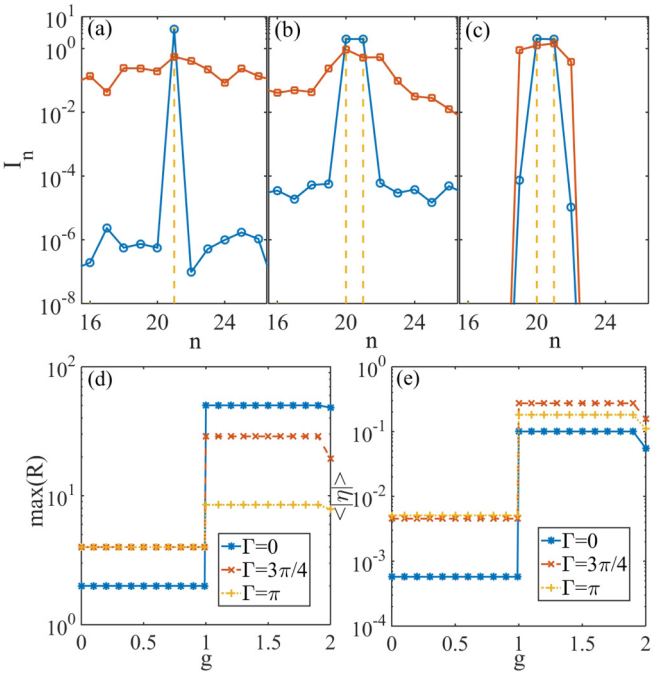

FIG. 3. Nonlinear delocalization and symmetry breaking of the CLS. (a–c) Intensity profiles $I_n = |a_n|^2 + |b_n|^2 + |c_n|^2$ at $z = 10\pi$ for $\Gamma = 0$ (a), $\Gamma = 3\pi/4$ (b), and $\Gamma = \pi$ (c). Cases when $g = 0.5$ and $g = 1$ are depicted with blue circle and red square symbol lines, respectively. Vertical dashed yellow lines mark the cell position of the input CLS. (d) Spreading of the CLS measured via the maximal value of the participation ratio R within the propagation length $z = 10\pi$. (e) z average of the normalized leg imbalance η.

corresponding instability eigenmodes share this compact localization but occupy more sites than the nonlinear CLS, as shown in Fig. 2(c). Now, the complex EV branches can be associated with oscillatory instabilities developed due to the mutual interactions among CLS components arising from different flatbands. Such oscillations involving multiple CLS are also observable in the linear case (see single "B"-site excitation in Ref. [7]) and are specific to AB cages.

IV. PROPAGATION DYNAMICS AND SYMMETRY BREAKING

Above, LSA describes the initial dynamics of a perturbed CLS, assuming all other modes remain weakly excited. This assumption is typically satisfied for resonant interactions between nonlinear localized modes and continua of low-amplitude dispersive waves, because the latter propagate away from the localized mode, stop interacting with it, and thereby preserve their low amplitude. This argument fails for AB cages because all low-amplitude modes are strictly localized; if linear instabilities exist, the unstable mode amplitudes will grow exponentially until nonlinear corrections become important. What then happens? This question cannot be resolved by the LSA and must be tackled using numerical simulations of the propagation dynamics.

Our central result, based on direct simulations of Eq. (1) taking CLS with random weak (5%) perturbations as the initial condition, is that the critical value $g = 1$ represents a bifurcation point beyond which nonlinear symmetry breaking of CLS occurs. This particular value of nonlinear parameter g separates a weak-instability regime from a strong-instability regime, regardless of the value of the synthetic magnetic flux Γ, illustrated by the examples in Figs. 3(a)–3(c). For even larger values of g (in the regions where LSA indicates stability), we observe a second transition to conventional self-trapping behavior for all values of Γ.

To characterize the transition at $g = 1$, we compute the normalized leg imbalance $\eta = \sum_n (|b_n|^2 - |c_n|^2)/P$ and the participation ratio $R = P^2/\sum_n (|a_n|^4 + |b_n|^4 + |c_n|^4)$. The former vanishes for all single band excitations; nonzero values indicate significant nonlinear interband coupling, enabling intensity-dependent phase shifts that break the AB cage by spoiling the destructive interference at the bottleneck sites. The participation ratio measures the number of sites occupied by the field, quantifying the wave-packet spreading.

As long as $g < 1$, the initially perturbed CLS evolves into a periodic breather, symmetric with respect to the A site and keeping almost of all of the total power within the initially excited nonlinear mode. Moreover, the dynamics are confined to the symmetric subspace, i.e., $|b_n| \approx |c_n|$ for all

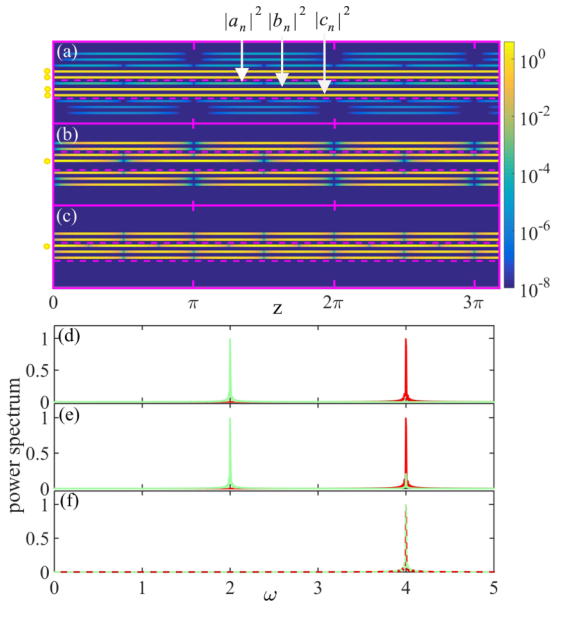

FIG. 4. Periodic dynamics of $\Gamma = \pi$ compact breathing modes in the weak-instability regime $g = 0.5$. (a–c) Evolution of compact breathing modes when the initial excitation condition is (a) CLS from $\beta_{FB} = 0$ submanifold, (b) single B site, and (c) single A site. Dashed purple lines mark edges of central unit cell, while yellow circles on the left denote excited sites at $z = 0$. Vertical axes schematically represent waveguides of the array. Each cell contains three waveguides (a, b, and c) marked in plot (a–c) for the general case of the nth cell. All plots contain the same number of cells. (d–f) Power spectra of the breathers in (a–c) obtained from Fourier transform of the site intensities $|a_n(z)|^2$ (red/dark gray) and $|b_n(a)|^2$ (green/light gray) in the central unit cell.

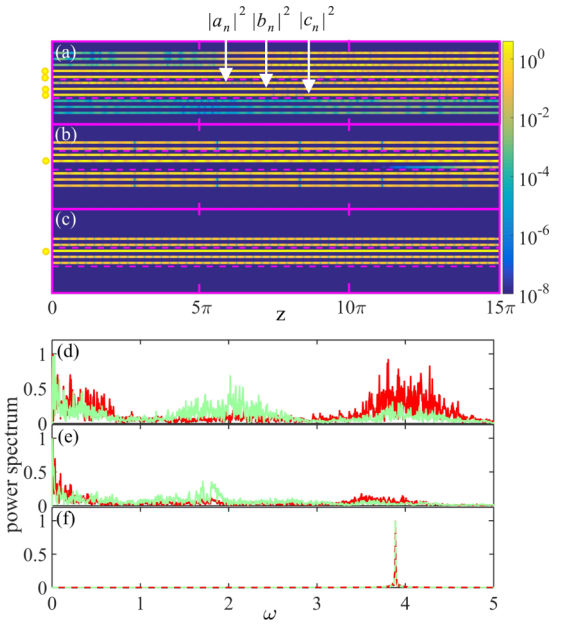

FIG. 5. Dynamics in the strong-instability regime $g = 1.9$ for the three different excitation conditions of Fig. 4. (a–c) z evolution exhibiting emergence of symmetry-broken profiles for the CLS and B excitations (a, b), while the A excitation remains symmetric. Vertical axes schematically represent waveguides of the array. Each cell contains three waveguides (a, b, and c) marked in plots (a–c) for the general case of the nth cell. (d–f) Corresponding power spectra of the intensities in the central unit cell.

z. Figures 3(d) and 3(e) show sudden increases of R and η occur at the bifurcation point $g = 1$. In this strong-instability regime, the breather loses stability and spreading becomes significant [red symbol lines in Figs. 3(a)–3(c)]. Although not affecting the precise bifurcation point, AB caging has an impact on R, which is smaller compared to the non-AB cage networks with $\Gamma \neq \pi$ due to the absence of delocalized linear modes.

This transition is not specific to the nonlinear CLS. We observe numerically similar nonlinear transitions for single-site excitations in the AB cage limit $\Gamma = \pi$. Figures 4(a)–4(c) show representative examples of the weak-instability regime for the CLS as well as B and A single-site excitations, revealing formation of periodic breathers. The corresponding power spectra in Figs. 4(d)–4(f) have sharp peaks corresponding to the energy difference between the flatbands. In particular, the single A-site excitation corresponds to a superposition of eigenmodes of the $\beta_{\pm} = \pm 2\kappa$ bands generating the breather oscillation frequency $\omega = 4$ [Fig. 4(f)]; there is no coupling into the $\beta_{FB} = 0$ flatband, and the symmetry between the two legs $\eta \approx 0$ is preserved.

In the strong-instability regime, a significant fraction of the power is coupled into other modes and the dynamics become aperiodic for the CLS and B-site excitations, as shown in Figs. 5(a), 5(b), 5(d), and 5(e). On the other hand, for $1 < g < 2$ the A-site excitation forms a different kind of five-site breather, with intensity oscillation frequency $\omega \approx 3.89$ independent of g. For $g \geqslant 2$ the system enters the self-trapping regime, where the dominant mechanism of localization is the nonlinearity rather than the intersite coupling [40]. In this case, the majority of the total power remains confined to the initially excited site regardless of Γ. Therefore, an excitation of bottleneck sites remains symmetric, regardless of the nonlinearity strength, due to the onset of self-trapping, whereas excitations of the legs can undergo the nonlinear symmetry breaking.

V. DISCUSSION AND CONCLUSION

The diamond network with properly tuned synthetic magnetic flux supports light localization analogous to AB caging in electronic systems. In the linear limit, destructive interference at bottleneck sites completely suppresses the spreading of localized excitations, leading to the existence of compact localized eigenstates. We showed that such eigenstates can persist as stable periodic breathers for sufficiently weak nonlinearities before undergoing a sudden symmetry-breaking transition at a critical nonlinearity strength. This symmetry breaking enables strong spreading of energy to neighboring cells, breaking the AB caging. We confirmed these statements using linear stability analysis and direct beam propagation simulations, observing that the symmetry-breaking transition is not sensitive to the precise strength of the effective magnetic flux. This transition occurring at finite nonlinearity strength is notably distinct from previous studies focusing on the

quantum limit, where all two-particle eigenstates become delocalized for arbitrarily weak interaction strengths.

Nonlinear breathers and symmetry breaking in AB cages are readily observable in femtosecond laser-written arrays similar to those in Refs. [7,21]. Previous experiments reported an effective nonlinear coefficient of $\gamma = 1.7\,\mathrm{cm}^{-1}\,\mathrm{MW}^{-1}$ with probe beam powers up to $P = 4$ MW [33]. Meanwhile, the AB cage experiment of Ref. [7] reported an effective coupling strength of $\kappa = 0.85\ \mathrm{cm}^{-1}$ with a propagation length $L = 10$ cm, corresponding to dimensionless propagation length $\kappa L = 8.5$ with normalized nonlinear coefficients $g = P\gamma/\kappa$ up to 8, sufficient to observe the three nonlinear regimes of weak instability, strong instability, and self-trapping.

Besides waveguide arrays, other possible platforms for observing nonlinear caging dynamics are Bose-Einstein condensates in optical lattices [41] and exciton-polariton condensates in structured microcavities [32]. In these cases, the governing equation is the Gross-Pitaevskii equation, which is equivalent to our Eq. (1) with the propagation distance z replaced by time t, and the optical field amplitude replaced by the mean-field condensate wave function [42]. These settings would furthermore allow exploration of the crossover from the mean-field limit studied here to the quantum many-body regime explored in Refs. [22–31].

Finally, we note that the underlying mechanisms we have explored here are rather general, relying only on the interplay between a synthetic magnetic flux and nonlinear phase shifts at bottlenecks in a tight-binding network. This can be readily generalized to two-dimensional AB cage structures such as the dice lattice, where additional nonlinear propagation regimes may emerge [17,25].

ACKNOWLEDGMENTS

We acknowledge support from the Ministry of Education, Science and Technological Development of the Republic of Serbia (Project No. III 45010) and the Institute for Basic Science in Korea (Grant No. IBS-R024-Y1).

[1] F. Nori and Q. Niu, Angular momentum irreducible representation and destructive quantum interference for Penrose lattice Hamiltonians, in *Quasi Crystals and Incommensurate Structures in Condensed Matter* (World Scientific, Singapore, 1990), p. 434.

[2] J. Vidal, R. Mosseri, and B. Douçot, Aharonov-Bohm Cages in Two-Dimensional Structures, Phys. Rev. Lett. **81**, 5888 (1998).

[3] Y. Aharonov and D. Bohm, Significance of electromagnetic potentials in the quantum theory, Phys. Rev. **115**, 485 (1959).

[4] R. G. Chambers, Shift of an Electron Interference Pattern by Enclosed Magnetic Flux, Phys. Rev. Lett. **5**, 3 (1960); Y. Gefen, Y. Imry, and M. Y. Azbel, Quantum Oscillators and the Aharonov-Bohm Effect for Parallel Resistors, *ibid.* **52**, 129 (1984); L. Duca, T. Li, M. Reitter, I. Bloch, M. Shleier-Smith, and U. Schneider, An Aharonov-Bohm interferometer for determining Bloch band topology, Science **347**, 288 (2014).

[5] D. L. Bergman, C. Wu, and L. Balents, Band touching from real-space topology in frustrated hopping models, Phys. Rev. B **78**, 125104 (2008).

[6] J.-W. Rhim and B.-J. Yang, Classification of flat bands according to the band-crossing singularity of Bloch wave functions, Phys. Rev. B **99**, 045107 (2019).

[7] M. Kremer, I. Petrides, E. Meyer, M. Heinrich, O. Zilberberg, and A. Szameit, Non-quantized square-root topological insulators: A realization in photonic Aharonov-Bohm cages, arXiv:1805.05209v1.

[8] C. C. Abilio, P. Butaud, Th. Fournier, B. Pannetier, J. Vidal, S. Tedesco, and B. Dalzotto, Magnetic Field Induced Localization in a Two-Dimensional Superconducting Wire Network, Phys. Rev. Lett. **83**, 5102 (1999).

[9] *Physics of Quantum Rings*, edited by V. M. Fomin (Springer-Verlag, Berlin, 2014); R. Saito, G. Dresselhaus, and M. S. Dresselhaus, *Physical Properties of Carbon Nanotubes* (Imperial College Press, London, 1998).

[10] O. V. Kibis, H. Sigurdsson, and I. A. Shelykh, Aharonov-Bohm effect for excitons in a semiconductor quantum ring dressed by circularly polarized light, Phys. Rev. B **91**, 235308 (2015).

[11] M. Hasan, I. V. Iorsh, O. V. Kibis, and I. A. Shelykh, Optically controlled periodical chain of quantum rings, Phys. Rev. B **93**, 125401 (2016).

[12] B. Doucot and J. Vidal, Pairing of Cooper Pairs in a Fully Frustrated Josephson-Junction Chain, Phys. Rev. Lett. **88**, 227005 (2002).

[13] B. Doucot, M. V. Feigel'man, L. B. Ioffe, and A. S. Ioselevich, Protected qubits and Chern-Simons theories in Josephson junction arrays, Phys. Rev. B **71**, 024505 (2005).

[14] M. Rizzi, V. Cataudella, and R. Fazio, $4e$-condensation in a fully frustrated Josephson junction diamond chain, Phys. Rev. B **73**, 100502(R) (2006).

[15] S. Gladchenko, D. Olaya, E. Dupont-Ferrier, B. Doucot, L. B. Ioffe, and M. E. Gershenson, Superconducting nanocircuits for topologically protected qubits, Nat. Phys. **5**, 48 (2009).

[16] M. T. Bell, J. Paramanandam, L. B. Ioffe, and M. E. Gershenson, Protected Josephson Rhombus Chains, Phys. Rev. Lett. **112**, 167001 (2014).

[17] G. Möller and N. R. Cooper, Synthetic gauge fields for lattices with multi-orbital unit cells: Routes towards a π-flux dice lattice with flat bands, New J. Phys. **20**, 073025 (2018).

[18] J. Jünemann, A. Piga, S.-J. Ran, M. Lewenstein, M. Rizzi, and A. Bermudez, Exploring Interacting Topological Insulators with Ultracold Atoms: The Synthetic Creutz-Hubbard Model, Phys. Rev. X **7**, 031057 (2017).

[19] K. Fang, Z. Yu, and S. Fan, Realizing effective magnetic field for photons by controlling the phase of dynamic modulation, Nat. Photon. **6**, 782 (2012).

[20] S. Longhi, Aharonov-Bohm photonic cages in waveguides and coupled resonator lattices by synthetic magnetic fields, Opt. Lett. **39**, 5892 (2014).

[21] S. Mukherjee, M. Di Liberto, P. Öhberg, R. R. Thomson, and N. Goldman, Experimental Observation of Aharonov-Bohm Cages in Photonic Lattices, Phys. Rev. Lett. **121**, 075502 (2018).

[22] G. Möller and N. R. Cooper, Correlated Phases of Bosons in the Flat Lowest Band of the Dice Lattice, Phys. Rev. Lett. **108**, 045306 (2012).

[23] R. Mondaini, G. G. Batrouni, and B. Gremaud, Pairing and superconductivity in the flat band: Creutz lattice, Phys. Rev. B **98**, 155142 (2018).

[24] J. Vidal, B. Douçot, R. Mosseri, and P. Butaud, Interaction Induced Delocalization for Two Particles in a Periodic Potential, Phys. Rev. Lett. **85**, 3906 (2000).

[25] J. Vidal, P. Butaud, B. Douçot, and R. Mosseri, Disorder and interactions in Aharonov-Bohm cages, Phys. Rev. B **64**, 155306 (2001).

[26] S. Takayoshi, H. Katsura, N. Watanabe, and H. Aoki, Phase diagram and pair Tomonaga-Luttinger liquid in a Bose-Hubbard model with flat bands, Phys. Rev. A **88**, 063613 (2013).

[27] M. Tovmasyan, E. P. L. van Nieuwenburg, and S. D. Huber, Geometry-induced pair condensation, Phys. Rev. B **88**, 220510(R) (2013).

[28] M. Tovmasyan, S. Peotta, L. Liang, P. Törmä, and S. D. Huber, Preformed pairs in flat Bloch bands, Phys. Rev. B **98**, 134513 (2018).

[29] C. Cartwright, G. De Chiara, and M. Rizzi, The Rhombi-chain Bose-Hubbard model: Geometric frustration and interactions, Phys. Rev. B **98**, 184508 (2018).

[30] O. Derzhko and J. Richter, Strongly correlated flat-band systems: The route from Heisenberg spins to Hubbard electrons, Int. J. Mod. Phys. B **29**, 1530007 (2015).

[31] D. Leykam, A. Andreanov, and S. Flach, Artificial flat band systems: from lattice models to experiments, Adv. Phys. X **3**, 1473052 (2018).

[32] F. Baboux, L. Ge, T. Jacqmin, M. Biondi, E. Galopin, A. Lemaitre, L. Le Gratiet, I. Sagnes, S. Schmidt, H. E. Türeci, A. Amo, and J. Bloch, Bosonic Condensation and Disorder-Induced Localization in a Flat Band, Phys. Rev. Lett. **116**, 066402 (2016).

[33] M. Heinrich, R. Keil, F. Dreisow, A. Tünnermann, A. Szameit, and S. Nolte, Nonlinear discrete optics in femtosecond laser-written photonic lattices, Appl. Phys. B **104**, 469 (2011).

[34] C. Danieli, A. Maluckov, and S. Flach, Compact discrete breathers on flat-band networks, J. Low Temp. Phys. **44**, 678 (2018).

[35] E. H. Lieb, Two Theorems on the Hubbard Model, Phys. Rev. Lett. **62**, 1201 (1989).

[36] A. Szameit, Y. V. Kartashov, F. Dreisow, M. Heinrich, T. Pertsch, S. Nolte, A. Tünnermann, V. A. Vysloukh, F. Lederer, and L. Torner, Inhibition of Light Tunneling in Waveguide Arrays, Phys. Rev. Lett. **102**, 153901 (2009).

[37] R. Keil, C. Poli, M. Heinrich, J. Arkinstall, G. Weihs, H. Schomerus, and A. Szameit, Universal Sign Control of Coupling in Tight-Binding Lattices, Phys. Rev. Lett. **116**, 213901 (2016).

[38] W. Maimaiti, A. Andreanov, H. C. Park, O. Gendelman, and S. Flach, Compact localized states and flat-band generators in one dimension, Phys. Rev. B **95**, 115135 (2017).

[39] P. P. Beličev, G. Gligorić, A. Maluckov, and M. Stepić, Dynamics of dark solitons localized at structural defect in one-dimensional photonic lattices with defocusing saturable nonlinearity, Europhys. Lett. **104**, 14006 (2013).

[40] A. B. Aceves, C. De Angelis, T. Peschel, R. Muschall, F. Lederer, S. Trillo, and S. Wabnitz, Discrete self-trapping, soliton interactions, and beam steering in nonlinear waveguide arrays, Phys. Rev. E **53**, 1172 (1996).

[41] G. Pelegri, A. M. Marques, R. G. Dias, A. J. Daley, J. Mompart, and V. Ahufinger, Topological edge states and Aharnov-Bohm caging with ultracold atoms carrying orbital angular momentum, arXiv:1807.08096.

[42] M. Liberto, S. Mukherjee, and N. Goldman, Nonlinear dynamics of Aharonov-Bohm cages, arXiv:1810.07641v1.